Original Article

Lithium ferrite (Li$_{0.5}$Fe$_{2.5}$O$_4$): synthesis, structural, morphological and magnetic evaluation for storage devices

Mukhtar Ahmad [a], Muhammad Shahid [a], Yousef Mohammed Alanazi [b], Atiq ur Rehman [c,], Muahmmad Asif [a,**], Charles W. Dunnill [d]*

[a] Department of Physics, COMSATS University Islamabad, Lahore Campus, 54000, Pakistan
[b] College of Engineering, Chemical Engineering Department, King Saud University Riyadh, Saudi Arabia
[c] Department of Physics, Riphah International University, Lahore Campus, Lahore, Pakistan
[d] Energy Safety Institute (ESRI), Swansea University Bay Campus, Swansea, SA1 8EN, UK

ARTICLE INFO

ABSTRACT

Lithium ferrite Li$_{0.5}$Fe$_{2.5}$O$_4$ has been synthesized by the use of the sol—gel technique. X-ray diffractometer (XRD) has been employed to confirm the crystal structure of spinel ferrites. No impurity peaks are detected in XRD graph, which confirms single phase crystal structure. The evaluation of grain size and analysis of external surface morphology of synthesized lithium ferrites has been done by scanning electron microscope (SEM). Average grain size was about equal to 131 nm. Energy dispersive x-ray spectra showed all the elements were present in required proportions. Magnetic characteristics such as saturation magnetization (M$_s$), remanence (M$_r$), and coercive force (H$_c$) have been measured from MH loops. Saturation magnetization has been measured to be 43.69 emu/by law of approach to saturation. The coercivity value lies in the range of few hundred Oersted which is vital condition for electromagnetic materials. Cyclic Voltammetry (CV) measurements were made, to know about the electrochemical performance of the material. CV results show that with the increase in scan rate specific capacitance decreases and the area of the loop increases which is promising for the formation of super capacitors and lithium-ion batteries (LIB's).

1. Introduction

Magnetic materials are being considered an interesting domain of research. This explicit study of substituted ferrites reflects that the properties of ferrites depend on the preparing conditions and modes being employed. Ferrites are ceramic materials, it looks like grey or black colors in appearance, and their profile is solid and brittle. Ferrites materials are magnetic

in nature and composed of metallic oxides comprising ferric ions as the central part and classified as magnetic material of ferrimagnetic nature [1]. These materials are very useful type of magnetic and electrical materials due to their high resistive force and minimum losses, excellencies in magnetic properties, and therefore have a wide range of technical applications. Ferrites have their own advantages; they can fabricate higher performance in low-cost material than any other material [1]. The ferrites, in fine particles or thin films form, can be synthesized by using, very high temperature solid-state [1], sol—gel [2], co precipitation [3], high energy ball milling [4], and hydrothermal [5] methods. The particles that are known to be of greater interest and their characteristics are being analyzed among them, are the nano-sized ferrites. Nano-sized ferrites have their own qualities for eloquent physical properties on a methods basis and are also known for technically designed applications. The physical uniqueness of nano-sized materials can commonly be regulated by grain boundaries as compared to a number of grains [6]. The electrical characteristics of the nano-size ferrites are being affected when the size of the particle reaches its critical size, and particles beneath this behave like a single domain [7]. Ferrites have a high value of permittivity which is of the order of thousand at smaller frequencies, falling to about 12—22 at microwave frequencies. This is just because of the packed arrangement of O_2 ions [8]. Commonly ferrites have either a smaller hysteresis loop area or square loop area [9]. Ferrites with smaller hysteresis envelop are categorized as soft ferrites and have tremendous applications in electric devices including transformers and solenoids of specific inductance. Ferrites having square loops are being categorized as hard ferrites that have applications in memory devices and automatically switching electronic devices. Ferrites have different types with respect to their structure for example Hexagonal, Spinel, Ortho, and Garnet. Specifically, the crystal structure of a spinel ferrite comprises two interstitial sites named tetrahedral "A" and octahedral "B". Cations can be accommodated at a tetrahedral "A" site and octahedral "B" site, enabling extensive variation in various properties of ferrites. Spinel ferrites are broadly examined for storage applications just because of their surface area, surface morphology, and porosity. As ferrites have high corrosion impedance and suitable conductivity, so they can be used as an electrode in storage cells. Lithium is a soft alkali metal of lightweight. It has one electron in its outermost shell so it has the smallest amount of ionization energy equal to 520 kJ/mol [9]. Lithium has a melting point of 179.55 °C, a boiling point of 1340 °C, a specific gravity of 0.55 (20 °C), and a valency of 1. Its density is approximately half that of water. It is an extremely reactive metal among all, it becomes stable if in the form of oxides, therefore it is an exceptional choice for making electrodes of a battery when mixed with ferrites. Due to high reactivity, it can produce a high voltage which is not possible by a conventional storage cell. Its energy density is 2.5—4.5 times greater than the conventional cells. Lithium based battery has a high operating range. It can work between −42 and 72 °C. As lithium has low ionization energy so it can easily be ionized and charging process can be initialized instantly. If we add lithium with ferrite then the conductivity of the material may increase. So, it is expected that lithium ferrites can offer maximum conduction and storage capacity,

high charging rate, and low discharging rate. Lithium ferrite has gained unusual attention due to its technological applications in microwave devices, magnetic recording tapes, transformer cores, etc [10]. It would be a promising nominee for electrode material in rechargeable lithium-ion batteries (LIB's). Lithium ferrite ($Li_{0.5}Fe_{2.5}O_4$) is promising material due to its importance in construction and engineering [10]. It can be crystallized in the spinel crystal structure, AB_2O_4, where "A" and "B" depicts lattice sites named as tetrahedral and octahedral supported by oxygen ions, respectively [11]. Bulk lithium ferrite ($Li_{0.5}Fe_{2.5}O_4$) has an inverse cations distribution of the form $(Fe^{3+})_a[Li_{0.5}Fe_{1.5}]_b$. The interplay between super exchange interactions of ferric ions (Fe^{3+}) ions at "A" and "B" sublattices gives rise to the ferrimagnetic alignment of magnetic domains, with a high Curie temperature (850K), and a saturation magnetization of about 72 Am^2/kg at room temperature [12]. Besides above mentioned many advantages, synthesis method plays a leading role, to accomplish excellent conductive and magnetic properties of the prepared ferrites for particular applications. There are many methods to prepare above said material but the sol—gel method is a simple method because it can be operated at low sintering temperature. The advantages of this method are low-cost precursor, easy to run, energy-efficient and the particles obtained by this method are nano-sized with fine structure. Main aim of this study is to study lithium ferrites ($Li_{0.5}Fe_{2.5}O_4$) for different applications for example synthesis of electrode for energy storage devices (LIB's), magnetic core inductors, camouflaging the military targets and multilayer chips in electronic devices etc.

2.   Material and Methods

2.1.   Synthesis techniques

Fine particle of lithium ferrite has been prepared by using sol—gel method. The sol—gel technique is a wet technique. It is frequently applied in material engineering as well as in ceramic engineering [13]. These methods are used mostly in material synthesis which begins from a solution of specific chemical composition, as these acts as precursor for an incorporated different material. These characteristic precursors are nitrates of metals and chlorides of the metals.

Analytical grades (sigma Aldrich 99.99%) of lithium nitrate and iron nitrate were dissolved in DI water. Citric acid as a chelating agent was added with 1:1. Temperature of solution was monitored by thermometer. pH of the solution was maintained by using solution of ammonia and it was monitored by using pH paper. Each solution was stirred on stirrer for 3 h separately. Mixture of solutions was stirred on the hot plate till the clear and homogeneous solution appeared. When pH is maintained, beaker was covered with the Aluminum foil and stirred on hot plate till the gel was formed. After that, this gel was collected and finally was poured onto the glass dish and gel was ready to be placed inside the oven for drying purpose. After drying ashes was collected and crushed to make the fine powdered by using mortar. For heat treatment powder was placed in a crucible and finally was sintered in a furnace at 700 °C for 7 h.

3. Results and discussion

3.1. X-ray diffraction

Structural characterization of the prepared lithium ferrite material was done by using Cu-K_α radiation having wavelength 1.5406 Å. Fig. 1 is showing the diffractogram of Lithium ferrite which is sintered at 700 °C for 7h and results are exactly matched with the previously reported results in literature [14]. By comparing with the previously reported literature, it has been proved that at high temperature, width of the central maxima decreased and as a result intensity is increased. This all is due to the increase in crystallite size at high temperature [15].

XRD patterns for lithium ferrite ($Li_{0.5}Fe_{2.5}O_4$) samples can be indexed to a crystalline structure of spinae by using powder diffraction file (PDF) no. 74-1911 mentioned in the standard of International Centre for Diffraction Data (ICDD), which basically belongs to space group $P4_132$ [16]. All diffraction peaks could be attributed to the reflections of (2 2 1), (2 2 0), (3 1 1), (3 1 7), (4 0 0), (4 2 2), (5 1 1), (4 1 9), and (4 4 0) planes which could be indexed to a face centered cubic (FCC) $Li_{0.5}Fe_{2.5}O_4$ ferrite. The XRD pattern has no extra peaks which means that material is single phased and has no impurity phase. By comparing results with literature, it proved that the crystallinity increases with sintering at high temperature and duration [17]. The lattice parameter for Lithium ferrite ($Li_{0.5}Fe_{2.5}O_4$) nano crystals prepared by sol—gel method was found to be 8.41 Å. Complete determination of an unknown crystal structure consists of three steps given below. Firstly, it involves computation of the number of atoms per unit cell from the size and shape of the unit cell, the chemical composition along with measured density. Secondly, deduction of the atomic positions within the unit cell and lastly calculation of the size and shape of the unit cell from the angular positions.

Average grain size was measured by using Debye Scherer's formula. Formula for calculating average crystallite size is given in Eq. (1), [18].

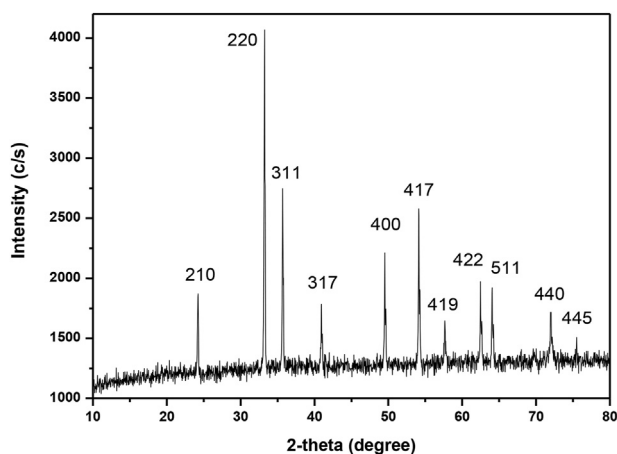$$D = \frac{0.9\lambda}{\beta \cos \theta} \quad (1)$$

Fig. 1 — XRD patterns for Lithium ferrites ($Li_{0.5}Fe_{2.5}O_4$).

In this case, D = Average crystallite size, β = Full width half maxima (220) and θ = Bragg's angle.

Scherer's formula gives average crystallite size provided that grain distribution is close and strain effects are negligible.

Apparent density was calculated by using Archimedes principle. It states that a body dipped (completely or partially) in a fluid is subjected to an upwards force equal to the weight of the displaced fluid. First of all determine the mass of pellet in air by using weight balance. Then measure the mass in water by Archimedes apparatus. Formula for Archimedes principle is given by Eq. (2) [18].

$$D_a = \frac{W_1}{Wx_1 - W_2} \times \rho \quad (2)$$

where w_1 is weight of pellet in air and w_2 is weight in water and ρ is the density of water.

Whenever Bragg's law is obeyed diffraction peak is appeared. Bragg's law is given by following formula.

$$n\lambda = 2d \sin \theta \quad (3)$$

The lattice constant (a) and volume (V) of the unit cell for single phase samples was calculated by using following formula 4 [19].

$$.sin^2 \theta = \frac{\lambda^2}{4a^2}\left(h^2 + k^2 + l^2\right) \quad (4)$$

where hkl are Miller Indices of each line, and θ is the Bragg angle. Miller indices can be evaluated by using following formula 5 [19].

$$d_{hkl} = \frac{a}{\sqrt{h^2 + k^2 + l^2}} \quad (5)$$

As Lithium ferrite is a cubic material so a = b = c. that's why following formula was used for the calculation of unit cell volume.

$$V = a^3 \quad (6)$$

It informs about the density of the atoms or molecules in a unit cell of a compound. The following equation was used to calculate the X-rays density [19].

$$.D_x = \frac{n \times M}{V \times Na} \quad (7)$$

here, n = number of molecules in a unit cell of spinel = 8, N_A = Avogadro's number (6.022×10^{23}), M = molecular weight.

Percentage porosity shows the extent of pores in the material. Porosity was calculated by using following relation and results are tabulated in Table 1 [18].

$$P\% = \frac{D_x - D_a}{D_x} \times 100 \quad (8)$$

The surface area in meter square per kilograms was obtained by using Eq. (9) [19].

$$S = \frac{6}{D \times D_B} \quad (9)$$

where "D" is diameter of nano particle in nanometers and 'D_B' is the bulk density of the grown particle in kg/m^3. (Note: If the 'D' is measured in nanometers and density is measured in g/cm^3 then "S" would become equal to $6000.0/D*D_B$).

Table 1 − Various Structural parameters of Lithium ferrites (Li$_{0.5}$Fe$_{2.5}$O$_4$).								
a (Å)	D (nm)	V (Å^3)	Dx (g/cm^3)	D$_B$ (g/cm^3)	Porosity %	S (g/m^2)	δ (lines/m^2)	ε (1/cm^2)
8.41	59.2	594.8	4.625	2.693	39%	37.622	2.85×10^{16}	2.05×10^{-3}

Dislocation density is a measurement of dislocations in the unit volume. Prepared material is polycrystalline. Dislocation density is measured in number of lines per unit area. It can be calculated by using following formula 10 [19].

$$\delta = \frac{1}{D^2} \tag{10}$$

D = Size of crystallite

3.1.1. Positional parameter

It is defined as "distance between any ion of oxygen at lattice points and face of the FCC of spinal ferrite". Positional parameter of oxygen increases from 0.3841 Å to 0.3861 Å. In an ideal FCC structure, value of positional parameter u = 0.375 [20]. The arrangements of ions of O^{-2} are closed packed cubic, but actual spinal structure is quite different from ideal structure. This is due to defects in the lattice. Values of the different geometrical quantities are represented in the table below. Inter atomic distances between the cation and cation (M−M) are represented by variables "b, c, d, e, f" and interatomic distance between the cation, anion (M−0) are represented by

$$a_{theo} = \frac{8}{3\sqrt{3}} \left[(r_A + R_\circ) + \sqrt{3}(r_B + R_\circ) \right] \tag{12}$$

3.2. EDX analysis

The element composition of prepared material was measured by using EDX technique in the range 0−20 keV. The EDX spectra (Fig. 3) for prepared sample, shows the presence of C, Li, Fe, O and concentrations were very close to the used elemental composition. It should be noticed that there are some peaks of carbon detected in EDX graph. These are due to ashes of the material, formed at the time of heat treatment. In EDX machine, detectors are calibrated to detect radiations of specific energy. Energy less than the calibrated value couldn't be detected by the detectors. X-rays produced by Lithium elements are very low energy so detection is not possible by the radiation detector. In the figure given below has been plotted and labeled in origin software. Numbers of moles of each element were calculated from EDX data by using following relation.

$$\text{Number of moles (Me)} = \frac{\text{Observed wt\% (Me)} \times \text{molecular wt of sample}}{\text{atomic weight of (Me)100} \times} \tag{13}$$

variables "p, q, r and s" (Fig. 2) and bonding angles are evaluated by using the numerical values of lattice constant (a) and positional parameter of oxygen (u). Results of distances from cation to cation and cation to anion are matched with the literature which shows that material is purely crystalline and suitable for future applications for example microwave devices and storage devices [18].

It was calculated by using following relation.

$$U = \left[(r_A + R_\circ) \left(\frac{1}{a\sqrt{3}} \right) + \frac{1}{4} \right] \tag{11}$$

R o = 1.32 Å, it is radius of oxygen ion.

r_A, r_B are ionic radius of the tetrahedral and octahedral sites respectively.

Different distance parameters such as a, b, c, d, e, f, p, q, r, s (Table 2) and bond angles θ_1, θ_2, θ_3 and θ_4 (Table 3) have been calculate using the standard formulas and tabulated as well.

3.1.2. Theoretical lattice parameter

Theoretical value of the lattice constant was measured by using following relation and experimental results were very close to the theoretical results. Results are tabulated in Table 4 [21].

The calculated numerical quantities for EDX analysis are given in Table 5. EDX spectra shows highly intense peak for Fe at 7 and 7.5 keV, relatively less intense peak for O at 1 keV and lowest intense peak for Li at 1.5 keV. This is due to lesser molecular weight of Li as compared to Fe and O. Careful examination of the results show that all the elements are present in their required proportions with no impurity. No of moles of each element has been calculated with 3.52, 2.23, and 0.61 mol for O, Fe and Li, respectively.

3.3. Scanning electron microscopy

SEM images are given below (Fig. 4) which were sintered at 700 °C for 7h. Different parameters for example grain size, surface area was calculated. All results are matched with the previously reported results. There are very small spacing's in SEM images which shows good adhesion of the substituted materials. According to the surface morphology these nano particles are forming cluster and there is homogenous distribution of the nano particles. These are pore less nano
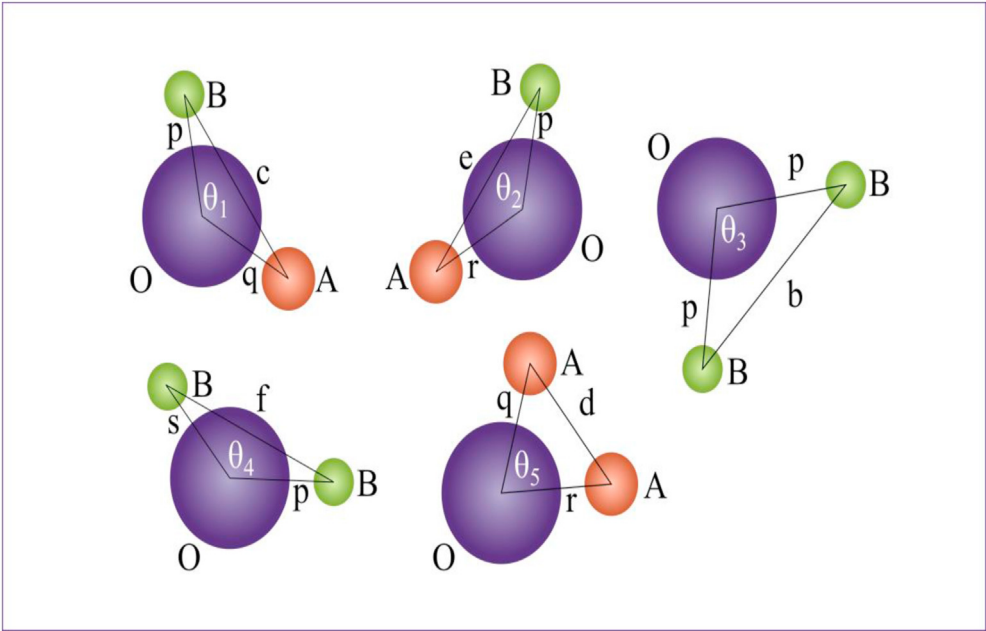
Fig. 2 – Configuration of the ion pairs in spinel ferrites with distances and angles.

Table 2 – Structural parameters of spinel ferrite.

Parameters	b	c	d	e	f	P	q	r	s
$Li_{0.5}Fe_{2.5}O_4$	2.97	3.49	3.64	5.46	5.15	2.0587	2.0165	3.640	3.657

Table 3 – Radius of octahedral and tetrahedral sites and Bond angles of spinel ferrite.

Parameters	$r_A(\text{Å})$	$r_A(\text{Å})$	θ_1	θ_2	θ_3	θ_4	θ_5
$Li_{0.5}Fe_{2.5}O_4$	0.6610	0.6999	125.6°	144.54°	93.01°	124.90°	72.87°

Table 4 – Theoretical and experimental Lattice parameters of Lithium ferrite.

Lattice Parameter	a_{theo}	a_{exp}
$Li_{0.5}Fe_{2.5}O_4$	8.49 Å	8.41 Å

Table 5 – Elemental composition for Lithium ferrites ($Li_{0.5}Fe_{2.5}O_4$).

Element	Atomic %	Weight %
O	57.143	50.03
Fe	35.714	37.88
Li	7.142	9.03

particles. Grain boundaries are not sharp because of low resolution. Image 'b' has high resolution. Dark color behind the nano spheres shows there is absence of nano material. Furthermore, the micrographs of the sample show well established single phase spinal ferrites. Single phase shape is the most acceptable shape for microwave absorption purposes. grain size measured by imagj software was131nm [22].

Mean size of the grain is measured by using **imagej software**. Mean size of grain was 131 nm. Maximum and minimum diameter of the grain was 186 nm and 92 nm respectively.

3.4. Magnetic properties

Fig. 5 shows hysteresis loop of lithium ferrite heat treated at $700^0$for interval of 7h. Literature shows that saturation
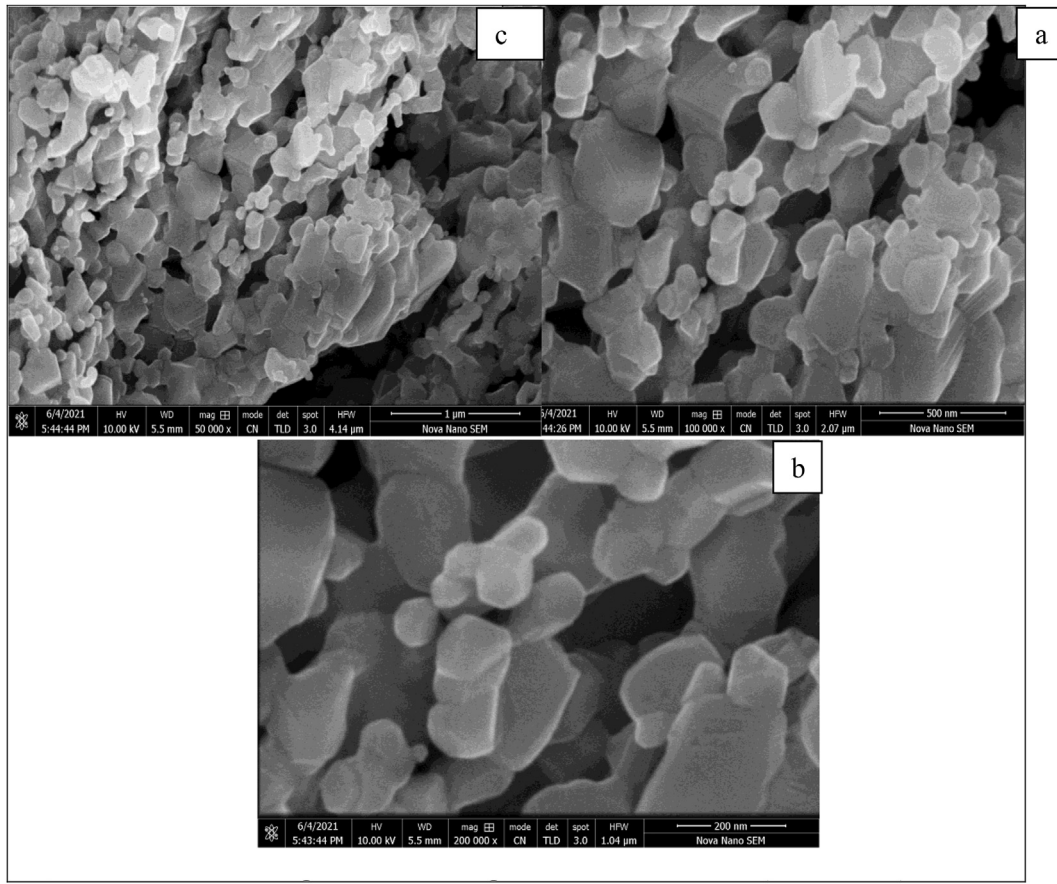

Fig. 3 – EDX spectra for Lithium ferrites ($Li_{0.5}Fe_{2.5}O_4$).

Fig. 4 — SEM images for Lithium ferrites ($Li_{0.5}Fe_{2.5}O_4$).

magnetization (M_S) affects with the change in temperature. It decreases by the increase in temperature. Change in saturation magnetization may be due to multi factors i.e. surface effects and redistribution of spins/cations and volatization of the lithium and oxygen. It is obvious from the hysteresis loop that the coercivity of prepared sample has value of few hundred oersted that means lithium ferrite is soft magnetic material [31]. Due to low vale of coercivity this material is excellent choice for making microwave and fast switching devices [23]. It is reported in the literature that porosity and
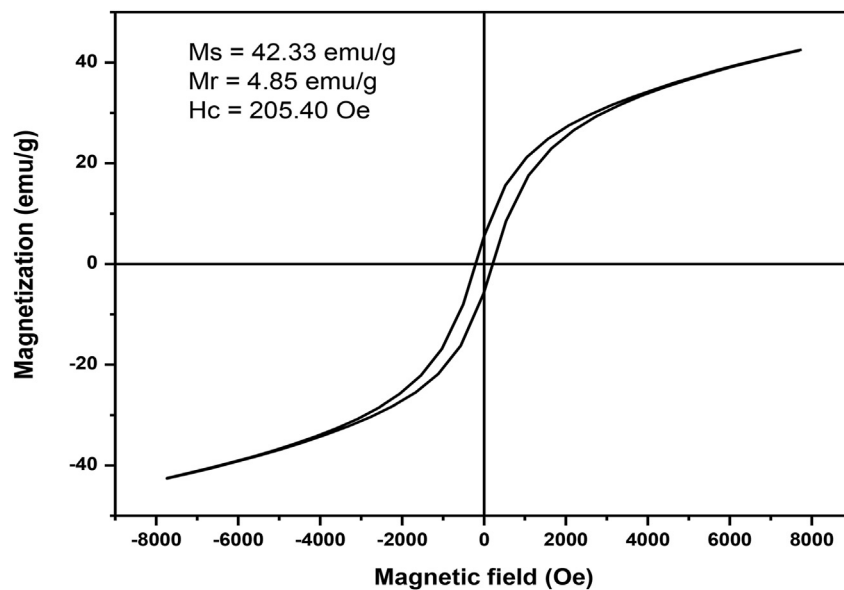

Fig. 5 — M—H loop for Lithium ferrites ($Li_{0.5}Fe_{2.5}O_4$).

size of the grain are the main factors that affects coercivity [26]. The loss in Li_2O results due to alpha iron oxide (Fe_3O_4) thereby reducing saturation magnetization. Porosity also decreases with the increase in firing temperature. The M−H loop for Lithium ferrites was achieved by applied field up to 8000Oe. M−H loop was used to find different magnetic characteristics of the sample, like saturation magnetization, retentivity, coercive force (H_c), magnetic moment, and ratio of (M_r/M_s) called as squareness ratio. Saturation magnetization (Ms) values were determined by using the law of approach (Loa) method in origin software [24].

To achieve the fitted data as shown in Fig. 6, saturation magnetization was measured by following rule known as least-squares process. Below formula was used in origin software to measure saturation magnetization [25].

$$M = M_s \left(1 - \frac{A}{H} - \frac{B}{H^2}\right) + \chi H$$

In above formula

M_s represents saturation magnetization.

A, represents an inhomogeneity constant

B represents factor which is proportional to square of the anisotropy constant (K^2).

H represents, Applied field.

χ represents magnetic Susceptibility.

Magnetic moment of the prepared material was also calculated by equation given below [26].

$$n_B(\mu_B) = \frac{Mw \times M}{5585}$$

where

M_w = molecular weight of the sample.

M = Saturation magnetized.

The saturation magnetization (M) and remanence (M_r) of sample have values of 42.33 emu/g and 4.85 emu/g, respectively. All values exactly matched with the already reported data. The magnetic moment (1.569) and coercivity of 205.4 Oe were observed for the sample (Table 6).

The anisotropic constant describes the measure of how different the transverse magnetization longitudinal magnetization is for an anisotropically magnetized medium. Results are tabulated in Table 6. It is represented by "k". Following formulae was used to calculate anisotropic constant [27,30].

$$K = \frac{H_c \times M_s}{0.96} \tag{14}$$

The magnetic anisotropic field depicts the hypothetical field which would be able to align all the magnetic moments perpendicular to easy axis. Results are tabulated in Table 6. Relation for magnetic anisotropic field and initial permeability is given by following formulas [30].

$$H_k = \frac{2K}{\mu_o \times M_s} \tag{15}$$

$$\mu_i = \frac{M_s^2 \times D}{K} \tag{16}$$

where

M_s = Saturation magnetization.

D = crystallite size.

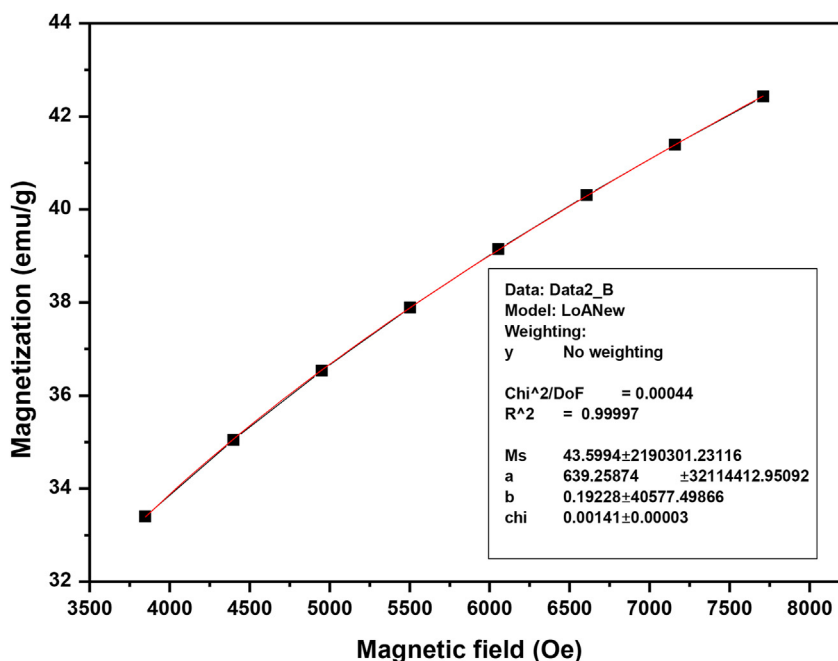

Fig. 6 − Fitted curves for by Law of approach (LoA).

Table 6 − Magnetic parameters of sol−gel synthesized Lithium ferrites ($Li_{0.5}Fe_{2.5}O_4$).								
Ms (emu/g)	Mr (emu/g)	Mr/Ms	n_B (μ_B)	Hc (Oe)	K (erg/g)	$H_{k\ (Oe)}$	χ	μ_i
42.33	4.85	0.12	1.569	205.40	9056.85	$34.07*10^7$	0.0014	11.734

μ_i = Initial permeability.

K = Anisotropy constant.

It should be noted that saturation by law of approach method is larger because it is calculated by higher value of the applied magnetic field.

As squareness ratio is less than 0.5 so, it represents that material is polly domain. Coercive force has value of the order of hundreds, so prepared material is best for microwave devices.

3.5. CV measurements

To test the electrochemical behavior of fabricated sample, cyclic voltammetry measurements were carried out at different scan rates, as 5 mV/s, 10 mV/s, 20 mV/s, 30 mV/s, 50 mV/s and 100 mV/s between the range of −0.2v to 1.0v in KOH electrolyte and $Li_{0.5}Fe_{2.5}O_4$ as electrode material. It can see in Fig. 7 that higher and lower peaks show the oxidation and reduction behavior respectively, which verify the electrochemical behavior of synthesized sample. When current values are increased by increasing scan rates, IR drop increased. During the cathodic reduction of iron, it transforms from Fe^{3+} to Fe^0. Curves reveal that noise increases with the increase in scan rate. Complete redox reaction equations are shown below.
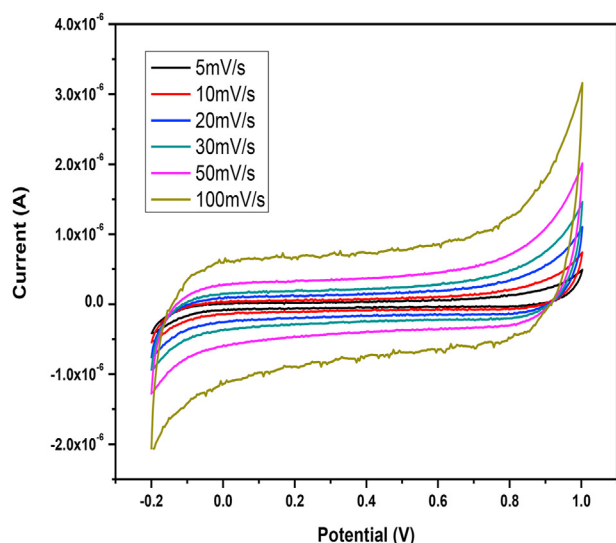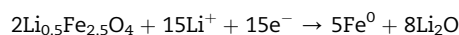
3.5.1. Cathodic reduction reaction

$$2Li_{0.5}Fe_{2.5}O_4 + 15Li^+ + 15e^- \rightarrow 5Fe^0 + 8Li_2O$$

3.5.2. Anodic oxidation reaction

After the completion of cycle, the cyclic voltametory curves are stable for the lithium ferrite nanoparticle which represents stability of electrode during the oxidation, reduction process. Area under the curve of V—I curve graph shows power rating of the battery. Complete reduction reaction is shown by equation given below.

$$2Fe^0 + 2Li_2O \rightarrow 2Fe^{II}O + 4Li^+ + 4e^-$$
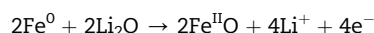
Literature shows that charge capacity is directly proportional to porosity of the sample. $Li_{0.5}Fe_{2.5}O_4$ has porosity of about 39% which means that it's a best material for storage devices.

3.6. Measurement of specific capacitance

Capacitance can be measured from CV curves by using following formula [28].

$$C_{cv} = \int_{v_i}^{v_f} \frac{I(V)dV}{2ma(v_f - v_i)} \tag{17}$$

here in this formula

A = Area of the loop = $\int_{v_i}^{v_f} \frac{I(V)dV}{1}$

a = scan rate

m = activated material mass which was 20×10^{-6}g,

V_f = final voltage.

V_i = initial voltage

$v_f - v_i$ = potential window.

From Table 7 it is obvious that with increasing the scan rate area of the curves is increasing and specific capacitance decreasing [29]. With the increase in scan rate there is very small decrease in specific capacitance. From the graph it is clear that positions of saturation peaks don't vary with scan rate and peaks are proportional to the root of scan rate. As a result we can conclude that material is promising for the formation of supper capacitors and storage batteries (LIB's).

Fig. 7 — Cyclic voltammetry (CV) curves of Lithium ferrites ($Li_{0.5}Fe_{2.5}O_4$).

Table 7 — Specific capacitance of sol—gel synthesized Lithium ferrites ($Li_{0.5}Fe_{2.5}O_4$).			
Scan rate ($Li_{0.5}Fe_{2.5}O_4$) a (mV/s)	Area under curve (VA)	Potential window $v_f - v_i$ (volts)	Specific capacitance (F/g)
5	1.3162×10^{-7}	1.2	0.5484
10	2.3888×10^{-7}	1.2	0.4975
20	4.4037×10^{-7}	1.2	0.4586
30	6.4407×10^{-7}	1.2	0.4472
50	10.277×10^{-6}	1.2	0.4281
100	19.188×10^{-6}	1.2	0.3996

4. Conclusion

Single phase lithium ferrite ($Li_{0.5}Fe_{2.5}O_4$) material is successfully synthesized by sol−gel method. Formation of the grain by this method is possible at low temperature. XRD analysis confirms the presence of spinal structure. The peaks are indexed; material is single phased and polycrystalline. Crystallite size of 59.22 nm is measured by XRD analysis. Lattice parameter of 8.41 Å. Distances between cations and anion and bond angles confirm the pure tetrahedral and octahedral geometry. Morphology of the sample was checked by SEM. Grain shows porous spherical surface morphology. Mean grain size was about 131 nm. EDX analysis of the sample shows the correct elemental composition of the material and peaks showed the presence of composite elements. Detection of lithium was not possible by x-ray detector because it is calibrated up to 6 keV and lithium falls below than that value. The coercivity (Hc) of the sample lays in the range of a few hundred, which is one of the necessary conditions for electromagnetic materials and makes these materials ideal for microwave devices, security, switching and sensing applications. Electrochemical measurements (CV measurements) i.e. high percentage of porosity and specific capacitance confirms that material is promising for storage devices i.e. Lithium Ion Batteries (LIB's) and supper capacitors.

Declaration of Competing Interest

Atiq ur Rehman reports administrative support was provided by Riphah International University - Lahore Campus. Atiq ur Rehman reports a relationship with Riphah International University - Lahore Campus that includes: employment.

Acknowledgement

REFERENCES

[1] Pointon A, Saull R. Solid state reactions in lithium ferrite. J Am Ceram Soc 1969;52(3):157−60.

[2] Hussain A, Abbas T, Niazi SB. Preparation of Ni1−xMnxFe2O4 ferrites by sol−gel method and study of their cation distribution. Ceram Int 2013;39(2):1221−5.

[3] Gul I, Ahmed W, Maqsood A. Electrical and magnetic characterization of nanocrystalline Ni−Zn ferrite synthesis by co-precipitation route. J Magn Magn Mater 2008;320(3−4):270−5.

[4] Widatallah HM, Berry FJ. The influence of mechanical milling and subsequent calcination on the formation of lithium ferrites. J Solid State Chem 2002;164(2):230−6.

[5] Yao L, Yuebin Xi, Yong Feng. Synthesis of cobalt ferrite with enhanced magnetostriction properties by the sol− gel−hydrothermal route using spent Li-ion battery. J Alloys Compd 2016;680:73−9.

[6] Anantharaman M, Geroge Mathew, Marry John Asha, Nair S Swapna, P A Joy, et al. Structural, magnetic and electrical properties of the sol-gel prepared Li0. 5Fe2. 5O4 fine particles. Dyuthi; 2006.

[7] Tabuchi M, Kazauki Ado, Hikari Sakaebe, Christian Masquelier, Hiroyuki Kageyama, Osamu Nakumura. Preparation of AFeO2 (A= Li, Na) by hydrothermal method. Solid State Ionics 1995;79:220−6.

[8] Prakash C, Baijal J. Dielectric behaviour of tetravalent titanium-substituted Ni-Zn ferrites. J Less Common Met 1985;107(1):51−7.

[9] Haque MM, Huq M, Hakim M. Thermal hysteresis of permeability and transport properties of Mn substituted Mg−Cu−Zn ferrites. J Phys Appl Phys 2008;41(5):55007.

[10] Goldman A. Crystal structure of ferrites. In: Handbook of modern ferromagnetic materials. Springer; 1999. p. 207−27.

[11] Hessien M. Synthesis and characterization of lithium ferrite by oxalate precursor route. J Magn Magn Mater 2008;320(21):2800−7.

[12] Fu Y-P, Cheng-Hsuing Lin, Chung-wein Liu, Yeong-Der Yao. Microwave-induced combustion synthesis of Li0. 5Fe2. 5O4 powder and their characterization. J Alloys Compd 2005;395(1−2):247−51.

[13] Haneda K, Miyakawa C, Kojima H. Preparation of high-coercivity BaFe12O19. J Am Ceram Soc 1974;57(8):354−7.

[14] Wang X, Lishing Gao, Li Li, Huagui Zheng, Zude Zhang, Weichao Yu, et al. Low temperature synthesis of metastable lithium ferrite: magnetic and electrochemical properties. Nanotechnology 2005;16(11):2677.

[15] Gupta N, Mukesh C. Dimri, Subash C. Kashyap, D.C. Dube. Processing and properties of cobalt-substituted lithium ferrite in the GHz frequency range. Ceram Int 2005;31(1):171−6.

[16] Sattar A, Agami W. Study of the physical and magnetic properties of Li0. 3Zn0. 4− xCaxFe2. 3O4 ferrite. J Alloys Compd 2010;496(1−2):341−4.

[17] Hagemann H, R G Synder, Peacock AJ, L. Mandelkern. Quantitative infrared methods for the measurement of crystallinity and its temperature dependence: polyethylene. Macromolecules 1989;22(9):3600−6.

[18] Vigneswari T, Raji P. Structural, magnetic and optical properties of Al-substituted nickel ferrite nanoparticles. Int J Mater Res 2018;109(5):413−21.

[19] Cullity B. Plane spacings, appendix 3 (A3-1). Lattice geometry, elements of X-ray diffraction. MI, USA: Addison−Wesley Publishing Company Inc.; 1978. p. 501.

[20] Balamurugan S, Manimekalai S, Prakash I. Synthesis, characterization and electrical properties of Li 2 NiFe 2 O 4/NiFe 2 O 4 nanocomposites. J Mater Sci Mater Electron 2017;28(24):18610−9.

[21] Abu-Elsaad N. Elastic properties of germanium substituted lithium ferrite. J Mol Struct 2014;1075:546−50.

[22] Ahmed M, Okasha N, Oaf M, Kershi RM. The role of Mg substitution on the microstructure and magnetic properties of Ba Co Zn W-type hexagonal ferrites. J Magn Magn Mater 2007;314(2):128−34.

[23] Pullar RC, Bdikin IK, Bhattacharya AK. Magnetic properties of randomly oriented BaM, SrM, Co2Y, Co2Z and Co2W hexagonal ferrite fibres. J Eur Ceram Soc 2012;32(4):905−13.

[24] Grössinger R. A critical examination of the law of approach to saturation. I. Fit procedure. Phys Status Solidi 1981;66(2):665−74.

[25] Danan H, Herr A, Meyer A. New determinations of the saturation magnetization of nickel and iron. J Appl Phys 1968;39(2):669−70.

[26] Waldron R. Infrared spectra of ferrites. Phys Rev 1955;99(6):1727.

[27] Rondinone AJ, Samia AC, Zhang ZJ. Characterizing the magnetic anisotropy constant of spinel cobalt ferrite nanoparticles. Appl Phys Lett 2000;76(24):3624−6.

[28] Lim C-S, Teoh KH, Liew CW, Ramesh S. Electric double layer capacitor based on activated carbon electrode and biodegradable composite polymer electrolyte. Ionics 2014;20(2):251—8.

[29] Subramanya B, Bhat DK. Novel eco-friendly synthesis of graphene directly from graphite using 2, 2, 6, 6-tetramethylpiperidine 1-oxyl and study of its electrochemical properties. J Power Sources 2015;275:90—8.

[30] A. Rehman, S.F. Shaukat, M.N. Akhtar, M. Ahmad. A study of structural, magnetic and various dielectric parameters of Ca-substituted W-type hexaferritesfor spplications at 1—6 GHz frequencies. J Electron Mater 2019. https://doi.org/10.1007/s11664-019-07515-w.

[31] A. Rehman, S.F. Shaukat, A.S. Haidyrah, M.N. Akhtar, M. Ahmad. Synthesis and investigations of structural, magnetic and dielectric properties of Cr-substituted W-type Hexaferrites for high frequency applications. J Electroceramics 2021;46:93—106.